ACS APPLIED MATERIALS & INTERFACES

Research Article

www.acsami.org

Stable Ferroelectric Perovskite Structure with Giant Axial Ratio and Polarization in Epitaxial $BiFe_{0.6}Ga_{0.4}O_3$ Thin Films

Zhen Fan,[†,‡] Juanxiu Xiao,[#] Huajun Liu,[†] Ping Yang,[§] Qingqing Ke,[†] Wei Ji,[‡] Kui Yao,*[,‡] Khuong P. Ong,[⊥] Kaiyang Zeng,[#] and John Wang*[,†]

[†]Department of Materials Science and Engineering, National University of Singapore, 9 Engineering Drive 1, Singapore 117575, Singapore

[‡]Institute of Materials Research and Engineering, A*STAR (Agency for Science, Technology and Research), 3 Research Link, Singapore 117602, Singapore

[#]Department of Mechanical Engineering, National University of Singapore, 9 Engineering Drive 1, Singapore 117575, Singapore

[§]Singapore Synchrotron Light Source, National University of Singapore, 5 Research Link, Singapore 117603, Singapore

[⊥]Materials Science & Engineering Department, Institute of High Performance Computing, 1 Fusionopolis Way, Singapore 138632, Singapore

Supporting Information

ABSTRACT: Ferroelectric perovskites with strongly elongated unit cells (c/a > 1.2) are of particular interest for realizing giant polarization induced by significant ionic off-center displacements. Here we show that epitaxial $BiFe_{0.6}Ga_{0.4}O_3$ (BFGO) thin films exhibit a stable super-tetragonal-like structure with twinning domains regardless of film thickness and substrate induced strain, evidenced with high resolution X-ray diffractometry (HR-XRD), transmission electron microscopy (TEM) and piezoresponse force microscopy (PFM). The origin of the structural stability of BFGO is investigated by the first-principles calculation. The ferroelectric properties of BFGO are studied by PFM, first-principles calculation and macroscopic polarization−electric field (P−E) hysteresis measurement. A giant ferroelectric polarization of ∼150 $\mu C/cm^2$ is revealed by the first-principles calculations and confirmed by experiments. Our studies provide an alternative pathway of employing Ga-substitution other than the extensively studied strain engineering to stabilize the supertetragonal structure in $BiFeO_3$-based epitaxial thin films.

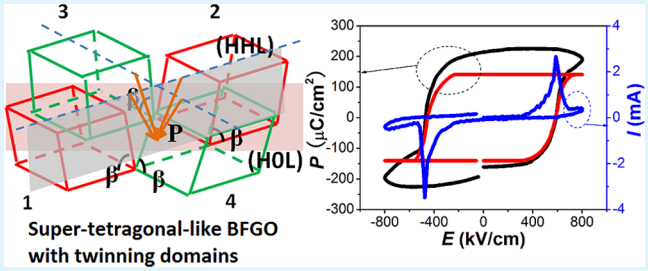

KEYWORDS: *$BiFeO_3$, supertetragonal, giant polarization, epitaxial thin film, ferroelectric*

1. INTRODUCTION

Ferroelectric thin films with large polarization are of great interest, not only for studying the physical mechanisms underlying the polarization,[1] but also for realizing high performance devices, such as actuators and sensors,[2] non-volatile memories,[3] and devices based on tunneling junctions[4] and bulk photovoltaic effect.[5] To achieve large polarization, perovskite-type oxides having super-tetragonal(-like) unit cells with giant c/a ratios (>1.2) are the ideal objects, due to the significant ionic displacements. One of the extensively studied routes to develop the supertetragonal structures is through epitaxial strain induced by the substrate.[6] For example, $BiFeO_3$ (BFO), which shows rhombohedral symmetry in its poly-crystalline bulk state, can be tailored to a supertetragonal structure with c/a ∼ 1.24 and a giant polarization of ∼150 $\mu C/cm^2$ under large compressive strains.[7−12] However, the strain-induced structure is often metastable, and it will relax toward its bulk when the film thickness exceeds certain value. Furthermore, when a bottom electrode has to be inserted between the substrate and the film for application, the strain effect is weakened and strain relaxation aggravates seriously. A recently demonstrated route is to stabilize supertetragonal BFO structures by the application of a β-Bi_2O_3 (β-BO) layer which facilitates the growth of supertetragonal BFO.[13,14] However, because β-BO is highly conductive and is likely to crystallize within the BFO layer, the leakage issue arises.[14]

It is well-known that formation of a solid solution can drastically tune the crystal structure and the physical properties, in comparison to the parent compositions, where $Pb(Zr_xTi_{1-x})O_3$ (PZT) is a classic example. In this letter, we demonstrate the stabilization of the desired super-tetragonal(-like) structure in BFO-based epitaxial thin films, by forming a Ga-substituted BFO solid solution, in contrast to the well-studied substrate strain approach. By using a combination of high resolution X-ray diffractometry (HR-XRD), transmission electron microscopy (TEM), piezoresponse force microscopy (PFM), first-

Received: November 4, 2014
Accepted: January 8, 2015
Published: January 8, 2015

DOI: 10.1021/am509016w
ACS Appl. Mater. Interfaces 2015, 7, 2648−2653

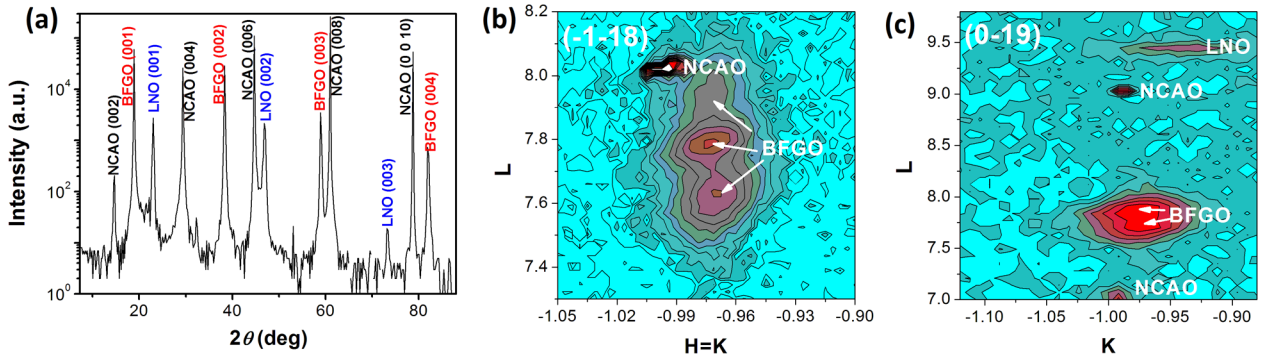

Figure 1. (a) X-ray diffraction θ–2θ scan of the 100 nm BFGO thin film grown on the LNO-buffered NCAO $(001)_{pc}$ substrate. Reciprocal space mappings around diffraction spots (b) (-1-18) and (c) (0-19) of the NCAO substrate, along with BFGO (-1-13) and (0-13), respectively.

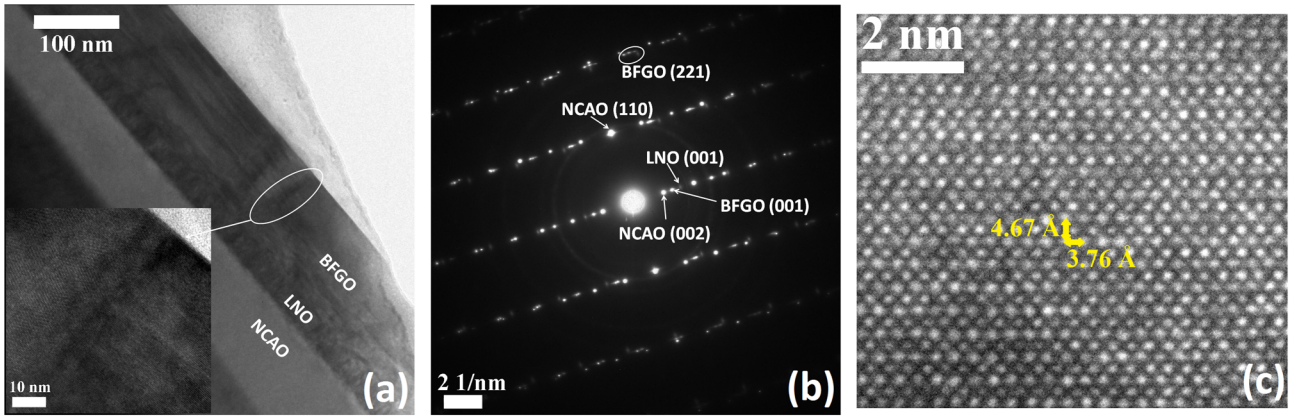

Figure 2. (a) Low magnification cross-sectional TEM image of BFGO/LNO/NCAO heterostructure with an inset showing the enlarged image of the boundary-like region. (b) SAED pattern taken along [-110] zone axis, where the split of BFGO (221) spots is indicated by the white circle. (c) High resolution TEM image of the BFGO super-tetragonal-like structure.

principles calculation and macroscopic polarization–electric field (P–E) hysteresis measurement, we show that $BiFe_{0.6}Ga_{0.4}O_3$ (BFGO) epitaxial thin films possess an intrinsically stable super-tetragonal-like structure with giant c/a ratios of ~1.25 and with twinning domains regardless of film thickness and substrate induced strain, together with a robust ferroelectricity (P_r ~ 150 $\mu C/cm^2$). We emphasize that although the super-tetragonal-like phase has already been reported in $BiFe_{1-x}Ga_xO_3$ powders[15] and polycrystalline thin films,[16] the epitaxial thin films have never been studied. In addition, the origin for the Ga-substitution induced structural stability of the supertetragonal phase was unclear. Therefore, the development of BFGO epitaxial thin films of super-tetragonal-like phase with giant c/a ratio is of particular interest, not only for the fundamental understanding of the Ga-substitution induced structural stability but also for their remarkable potentials in device applications.

2. EXPERIMENTAL PROCEDURE

A previous study[15] has demonstrated that super-tetragonal-like structures could be formed in $BiFe_{1-x}Ga_xO_3$ polycrystalline powders with $0.4 \leq x \leq 0.5$. To develop epitaxial thin films by sputtering, it has, however, been unsuccessful to obtain a sintered ceramic target with high levels of Ga concentration due to the severe cracking in association with phase instability upon sintering at ambient pressure. Therefore, our investigation is focused on the composition with Ga 40% in the present study. The ceramic target was made by sintering of the powder mixture of Bi_2O_3, Fe_2O_3 and Ga_2O_3 with mole ratio of 1.1:0.6:0.4 at 830 °C for 2 h. Epitaxial BFGO thin films of ~100 nm in thickness were grown on $(001)_{pc}$ $NdCaAlO_4$ (NCAO) substrates by radio frequency (RF) sputtering at 610 °C. The gas pressure was kept at 15 mTorr ($Ar:O_2$ = 14:13) during deposition. Prior to the deposition of BFGO thin films, a $LaNiO_3$ layer with the thickness of 30 nm was deposited as the bottom electrode. The composition of resulting BFGO thin films was analyzed by X-ray photoelectron spectroscopy (XPS) with a Kratos Axis Ultra X-ray photoelectron spectrometer (Kratos Analytical). The crystal structures of resulting BFGO thin films were studied by HR-XRD at the X-ray development and demonstration (XDD) beamline of Singapore Synchrotron Light Source (SSLS). Cross-sectional TEM images and selected-area electron diffraction (SAED) patterns were taken by using Philips CM300 FEG TEM. In the PFM study, a SPM system (MFP-3D, Asylum Research, USA) with a software platform (IGOR PRO 6.12A) and SPM control software (Asylum Research, version 090909-1214) was used. A commercially available Pt-coated Si tip (AC240TM, Olympus, Japan) with average tip radius of 15 nm, average stiffness of 2 N/m and average resonance frequency of 70 kHz was employed. The local ferroelectric hysteresis loops were measured by using piezoresponse force spectrosopy (PFS). The ferroelectric P–E loops were measured by Radiant Precision Premier II (Radiant Technologies). We performed the first-principles calculations using the PBE-GGA as implemented in the Vienna Ab initio Simulation Package (VASP), which employs the Projected Augmented Wave (PAW) method. A 3 × 3 × 3 Monkhorst–Pack k-mesh and an energy cutoff of 500 eV for plane waves were used. In the calculations, all atoms in the BFGO system were fully relaxed until the Hellmann–Feynman forces were less than 20 meV/Å.

DOI: 10.1021/am509016w
ACS Appl. Mater. Interfaces 2015, 7, 2648–2653

3. RESULTS AND DISCUSSION

A. Unique Super-Tetragonal-like Structure with Twinning Domains. As can be seen from the analytical XPS results (Table S1, Supporting Information), the atomic ratio of Bi:Fe:Ga = 1:0.60:0.41, which is consistent with the nominal value. Figure 1a shows the HR-XRD θ–2θ scan of the BFGO/LNO/NCAO heterostructure. The distinct and sharp peaks of BFGO, LNO and NCAO in the pattern suggest the formation of a single-phase thin film and the high-quality epitaxy in $(001)_{pc}$ orientation. A low magnification cross-sectional TEM image (see Figure 2a) shows sharp interfaces of LNO/NCAO and BFGO/LNO and a smooth surface of BFGO, which further confirms the high quality of the BFGO/LNO/NCAO heterostructure.

From the diffraction angles shown in Figure 1a, the d spacing of BFGO $(001)_{pc}$ is measured to be ~4.67 Å which is comparable to the reported super-tetragonal(-like) BFO.[7−14,17] The reciprocal space mappings (RSMs) around (-1-18) and (0-19) of the substrate NCAO are shown in Figure 1b,c, respectively. Interestingly, the (-1-18) HHL mapping shows a vertical splitting of BFGO (-1-13) peak into three peaks (Figure 1b). The splitting is due to the coexistence of four twinning variants with monoclinic tilts along $[110]_{pc}$, $[-110]_{pc}$, $[1-10]_{pc}$ and $[-1-10]_{pc}$ directions, respectively (see Figure 3a,b). If a

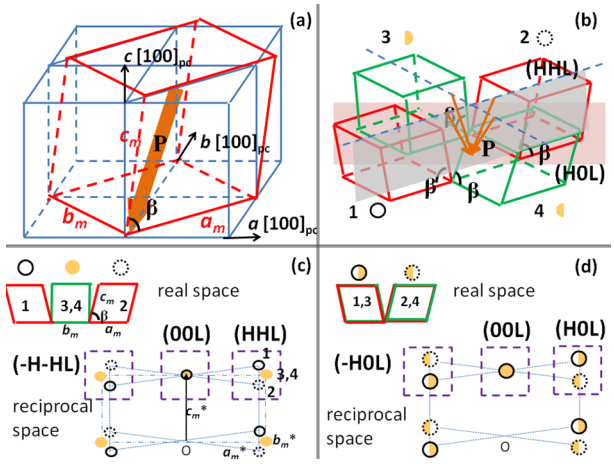

Figure 3. Schematics showing (a) the BFGO unit cell and (b) the configuration of four twinning variants. The reciprocal relationships between real lattice and reciprocal lattice for (c) (HHL) mapping and (d) (H0L) mapping.

diagonal plane passing the origin is used to cut through the real space, it will result in three sets of lattice. Variants 3 and 4 overlap completely, whereas variants 1 and 2 tilt toward different directions. Therefore, there will be three peaks of BFGO in (HHL) and (-H-HL) RSMs, as illustrated in Figure 3c. In addition, the middle peak of BFGO in Figure 1b has a stronger intensity than the other two because it is the diffraction of the two twinning variants together. The split of BFGO (HHL) spots is also observed in the SAED pattern taken along [-110] zone axis, as shown in Figure 2b. On the other hand, the two peaks of BFGO (0-13) shown in Figure 1c provide another evidence for the twinning structures. The cutting plane perpendicular to b-axis gives rise to two sets of lattice in the real space. Variant 1 overlaps with variant 3 and variant 2 overlaps with variant 4, respectively. This leads to two peaks with nearly the same intensity in (H0L) and (-H0L) RSMs (or (0KL) and (0-KL)), as shown in Figure 3d. The lattice parameters of the monoclinic unit cell are calculated as a_m = 5.338 Å, b_m = 5.319 Å, c_m = 4.694 Å and β = 91.98°. In accordance with the pseudocubic unit cell, the in-plane lattice constants are determined: $a \approx b \approx$ 3.768 Å and the c/a ratio is ~1.25. High resolution TEM further confirms the lattice parameters of the BFGO structure (see Figure 2c). These results are also consistent with the monoclinic C_m structures reported for BFGO in the forms of powder[15] and polycrystalline thin film.[16] One interesting point is that the super-tetragonal-like BFGO exhibits a monoclinic A-type (M_A) tilt, whereas BFO with similarly giant c/a ratio shows a monoclinic C-type (M_C) tilt.[9] However, M_A-BFO unit cell only possesses a much smaller c/a ratio of ~1.[9]

To further verify the twinning domain structures of BFGO, both TEM and PFM techniques were employed. We have observed boundaries (or boundary-like regions) between twinning domains in the low magnification cross-sectional TEM images (see Figure 2a). In addition, Figure 4a shows the out-of-plane (OP) PFM phase image with homogeneous contrast, suggesting that the BFGO sample is self-polarized and all the OP polarizations point to the same direction. Because the OP polarization could be reversed by applying a negative tip bias, the direction of the OP polarization in the as-grown state is downward (see Figure S1 in the Supporting Information). However, in the in-plane (IP) PFM phase images (both $IP_{[100]}$ and $IP_{[010]}$; see Figure 4b,c), the yellow-purple contrasts are observed, which indicates that the IP polarizations have two different orientations along both $[100]_{pc}$ and $[010]_{pc}$ directions. These results suggest the coexistence of four polarization variants (Figure 3b), which is consistent with the finding of HR-XRD. Combining $IP_{[100]}$ and $IP_{[010]}$ phase images, one can distinguish those four domains and map their distribution, as shown in Figure 4d. The chaotic domain patterns shown in the IP phase image were also reported for the supertetragonal BFO thin films.[10] The ferroelectric domains were further evidenced to be switchable by the PFS study. As shown in Figure 4e, the phase loop with a sharp ~180° domain switching and the amplitude loop with the shape of butterfly fully demonstrate the ferroelectric nature of the BFGO thin film in the nanoscale. The voltage offset of the amplitude butterfly loop is due to the internal field, which originates from the asymmetric distribution of trapped charge carriers.

B. Experimental Evidence of the Structural Stability. It is known that the supertetragonal BFO phase is largely metastable. However, we demonstrate that the super-tetragonal-like structure with twinning domains in BFGO thin films is considerably stable, both experimentally and theoretically. First, we increased the thickness of BFGO thin films to ~200 nm. Interestingly, as shown in Figure S2 (Supporting Information) and Figure 5a, the relative peak intensity of the 200 nm BFGO film becomes stronger than that of the 100 nm film, and the peak splitting is clearly observed, indicating that the super-tetragonal-like structure of BFGO with twinning domains is well retained. This thickness independent structural behavior of BFGO is essentially different from that of BFO, which shows a gradual relaxation from the supertetragonal structure toward the rhomhohedral-like structure as film thickness increases.[11,12,17] Next, the 100 nm BFGO thin films were directly grown on top of the NCAO and $SrTiO_3$ (STO) substrates, where the nominal epitaxial strains provided by those substrates were different (Note that the in-plane lattice constants of BFGO, LNO, NCAO are 3.768, 3.839, 3.905 and

DOI: 10.1021/am509016w
ACS Appl. Mater. Interfaces 2015, 7, 2648−2653

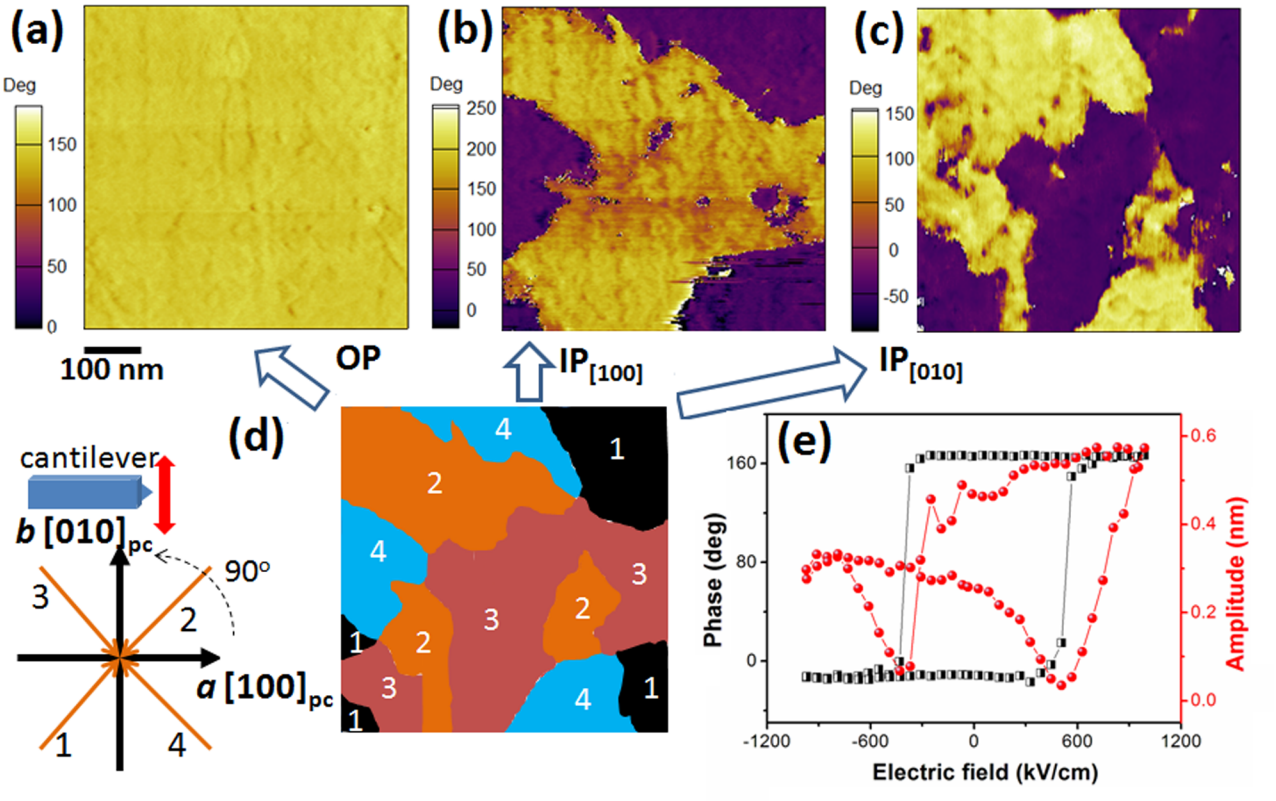

Figure 4. (a) OP and (b) $IP_{[100]}$, and (c) $IP_{[010]}$ phase images of the as-grown BFGO thin film, taken along $[001]_{pc}$, $[100]_{pc}$ and $[010]_{pc}$ directions, respectively. Images of a, b and c were taken at the same position of the sample. (d) Distribution of four domains. The left panel in d shows that the scanning of IP phase images along different directions was realized by rotating the sample. (e) OP phase and amplitude hysteresis loops.

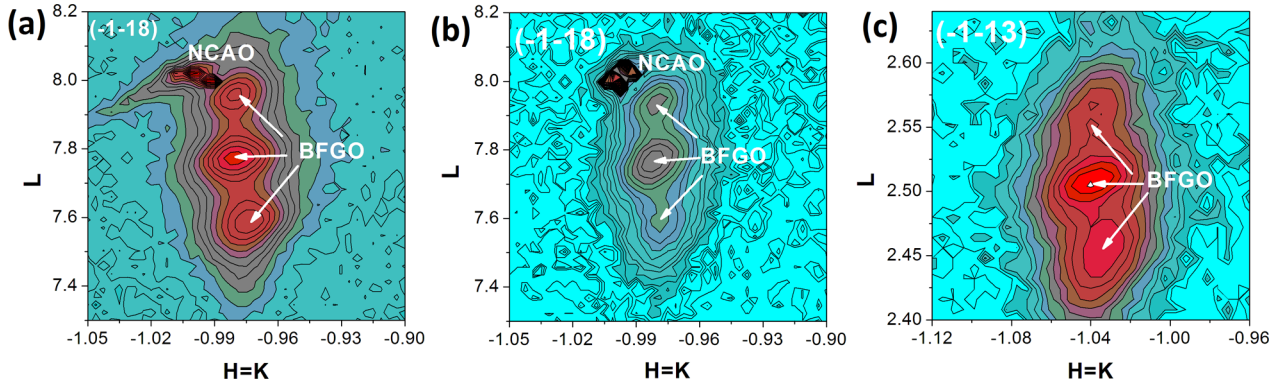

Figure 5. Reciprocal space mappings around the diffraction spots of NCAO (-1-18) and BFGO (-1-13) of (a) 200 nm BFGO film grown on the LNO-buffered NCAO substrate, and (b) 100 nm BFGO film directly grown on the NCAO substrate. (c) Reciprocal space mapping around the diffraction spot of BFGO (-1-13) of the 100 nm BFGO film directly grown on the STO substrate.

3.685 Å, respectively). Nevertheless, by comparing results shown in Figure 1b and 5b,c, one can see that the super-tetragonal-like structure of BFGO is retained on the substrates with a wide range of in-plane lattice constants through the partial (or full) relaxation of epitaxial strain.

C. First-Principles Studies of the Structural Stability and the Ferroelectricity. We have then performed first-principles calculations to investigate the most stable structure and corresponding ferroelectric polarization of BFGO. We built both tetragonal and rhombohedral BFGO structures by using 2 × 2 × 2 BFO supercells with 50% Fe atoms replaced by Ga atoms. Note for computational simplicity, the ratio x of $BiFe_{1-x}Ga_xO_3$ was approximated to be 0.5, instead of 0.4 in the real compound. We considered all possible configurations of Fe/Ga atoms and magnetic orderings of Fe atoms (see Table 1).

From Table 1, we find that the supertetragonal structure with a layer sandwiched structure between the Fe-layer and Ga-layer along the *c*-direction and with antiferromagnetic structure along the $[110]_{pc}$ direction is the most stable structure. Because Ga tends to form highly distorted coordination polyhedron,[15] the supertetragonal structure where one apical Ga−O bond is strongly elongated is energetically favored for BFGO. By allowing the monoclinic tilt of the out-of-plane axis along the face diagonal direction, the energy of the BFGO system is further decreased by ∼37 meV per formula unit, and the

DOI: 10.1021/am509016w
ACS Appl. Mater. Interfaces 2015, 7, 2648−2653

Table 1. Relative Energies of All Tetragonal and Rhombohedral Structures with Different Configurations of Fe/Ga Atoms and Spin Orderings of Fe Atoms[a]

structure	relative energies (meV per f.u.)	structure	relative energies (meV per f.u.)
T- Fe (001) - FM	133.2	T- Fe (110) - AFM [-111]	49.7
T- Fe (001) - AFM [010]	122.4	T- Fe (011) - FM	87.1
T- Fe (001) - AFM [110]	0	T- Fe (011) - AFM [100]	76.8
T- Fe (100) - FM	86.7	T- Fe (011) - AFM [01-1]	24.8
T- Fe (100) - AFM [010]	77.9	T- Fe (011) - AFM [11-1]	20
T- Fe (100) - AFM [001]	19.1	T- Fe (-111) - FM	74.8
T- Fe (100) - AFM [011]	22.2	T- Fe (-111) - AFM [110]	60.3
T- Fe (110) - FM	71.4	T- Fe (-111) - AFM [101]	727.5
T- Fe (110) - AFM [-110]	68.1	R- Fe (-111) - FM	164.3
T- Fe (110) - AFM [001]	49	R- Fe (-111) - AFM [110]	141.9

[a]The naming rule of all structures is described in Figure S5 (see the Supporting Information).

monoclinic C_m symmetry is obtained. The oxygen octahedra show in-phase tilts about *a* and *b* axes, and no tilts about *c*-axis, i.e., $a^+a^+c^0$ (see Figure 6). The tilts of the oxygen octahedra are

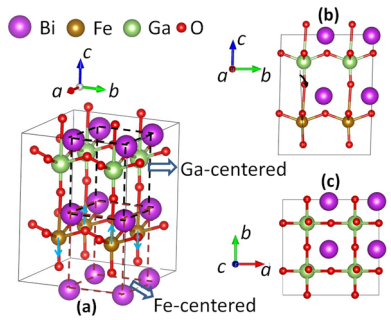

Figure 6. Most stable BFGO structure with C_m symmetry viewed from different directions: (a) an arbitrary axis, (b) *a*-axis and (c) *c*-axis. The small blue arrows in panel a indicate the spin directions of Fe atoms. The black arrow in panel b indicates the tilting direction of oxygen octahedra.

to accommodate the monoclinic lattice distortion and help to stabilize the BFGO system. Therefore, by theory, we demonstrate that the monoclinic-tilted supertetragonal structure is the most stable one for BFGO. Because there are four possibilities of monoclinic tilts along face diagonal directions, i.e., $[110]_{pc}$, $[-110]_{pc}$, $[1\text{-}10]_{pc}$ and $[\text{-}1\text{-}10]_{pc}$, one natural consequence is the formation of four twinning variants, which is consistent with our experimental observations.

Then, the ferroelectric polarization of the most stable C_m structure was calculated by both Berry phase[18,19] and Born effective charge methods.[20,21] The overall polarization is calculated to be (21.2, 21.2, 145.5) $\mu C/cm^2$ (the magnitude is ~150 $\mu C/cm^2$), by employing the Berry phase method. To further analyze the contribution from each ion, the Born effective charge method was used. As shown in Table 2, the in-plane polarization mainly comes from the Bi ion. Interestingly, the Ga ion is found to contribute much more toward the out-of-plane polarization, as compared with the other B-site ion, Fe. Therefore, the substitution of Fe by Ga is an effective way to enhance the ferroelectric polarization.

D. Macroscopic *P*–*E* Hysteresis Loop. We understand that it is difficult and challenging to quantify the large ferroelectric polarization predicted for the pure super-tetragonal-like phase at room temperature by the conventional *P*–*E* hysteresis measurement, due to the large coercive field and large leakage current at high electric field.[10] Although the giant

Table 2. Individual Contributions from Bi, Ga, and Fe Ions Toward Polarization

location of 5-atom unit cell	ion	polarization ($\mu C/cm^2$) P_x // $[100]_{pc}$	P_y // $[010]_{pc}$	P_z // $[001]_{pc}$
Ga-centered	Bi	24.6	24.6	69.4
	Ga	2.6	2.6	63.9
Fe-centered	Bi	23.3	23.3	80.7
	Fe	3.1	3.1	47.4

ferroelectric polarization of the super-tetragonal-like phase has been experimentally measured in a few of previous studies, those experiments were however conducted either at low temperature[13] or for a mixture of tetragonal and rhombohedral phases.[11,16] Nevertheless, by using Au top electrodes with a small area of 60 × 60 μm^2, we successfully reduced the influence of leakage current and obtained a macroscopic *P*–*E* hysteresis loop with a proper shape at room temperature, as shown in or Figure 7. By further deducting the leakage current,

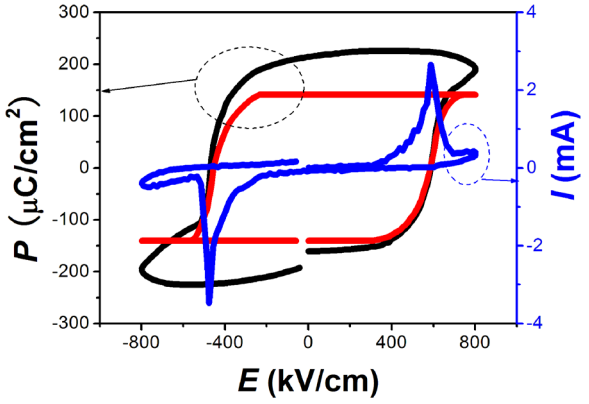

Figure 7. Macroscopic *P*–*E* (the black curve corresponds to raw data whereas the red curve corresponds to the *P*–*E* loop after subtracting leakage contribution) and corresponding current-field (*I*–*E*) hysteresis loops. A frequency of 10 kHz was used for the measurement.

the intrinsic P_r is revealed to be close to ~150 $\mu C/cm^2$, which is consistent with our first-principles calculation. It should be highlighted that this is the first time to successfully measure the predicted giant polarization of pure super-tetragonal(-like) phase at room temperature by the conventional *P*–*E* hysteresis measurement.

DOI: 10.1021/am509016w
ACS Appl. Mater. Interfaces 2015, 7, 2648–2653

4. CONCLUSIONS

In summary, a super-tetragonal-like structure with giant c/a ratio of ~1.25 and with twinning domains was developed in the BFGO epitaxial thin film grown on the NCAO $(001)_{pc}$ substrate with a LNO buffer layer. This unique structure was evidenced to be stable for the BFGO epitaxial thin films irrespective of film thickness and substrate induced strain, as confirmed by using multiple analytical techniques including HR-XRD, TEM and PFM, and further supported by the first-principles calculation. In addition, PFM studies, first-principles calculation and macroscopic $P-E$ hysteresis loop demonstrated the ferroelectric nature of BFGO and revealed a giant polarization of ~150 $\mu C/cm^2$. Ga-substitution is therefore shown to be an effective pathway to stabilize the super-tetragonal structure in the BFO-based ferroelectric epitaxial thin films.

■ ASSOCIATED CONTENT

Supporting Information

OP and IP PFM phase image after poling (Figure S1), XRD results of 200 nm BFGO film grown on the LNO-buffered NCAO substrate (Figure S2), 100 nm BFGO film directly grown on the NCAO substrate (Figure S3), and 100 nm BFGO film directly grown on the STO substrate (Figure S4), naming rule of all possible BFGO structures (Figure S5), and analytical XPS results (Table S1). This material is available free of charge via the Internet at http://pubs.acs.org.

■ AUTHOR INFORMATION

Corresponding Authors

*K. Yao. E-mail: k-yao@imre.a-star.edu.sg.
*J. Wang. E-mail: msewangj@nus.edu.sg.

Notes

The authors declare no competing financial interest.

■ ACKNOWLEDGMENTS

Z.F. and J.W. acknowledge the support from the Agency for Science, Technology and Research (A*Star) for research (Grant number: 1121202013), conducted at the National University of Singapore. The authors from IMRE acknowledge the support from Institute of Materials Research and Engineering, A*STAR, and through project IMRE/10-1C0107. P.Y. acknowledges the support from SSLS via NUS Core Support C-380-003-003-001. K.P.O. acknowledges the support from Institute of High Performance Computing (IHPC) A*STAR. K.Z. is supported by National University of Singapore and Ministry of Education of Singapore under the Academic Research Funding (Grant No. R265-000-257-112).

■ REFERENCES

(1) Uratani, Y.; Shishidou, T.; Ishii, F.; Oguchi, T. First-Principles Predictions of Giant Electric Polarization. *Jpn. J. Appl. Phys.* **2005**, *44*, 7130−7133.
(2) Muralt, P. Ferroelectric Thin Films for Micro-sensors and Actuators: A Review. *J. Micromech. Microeng.* **2000**, *10*, 136−146.
(3) Dawber, M.; Rabe, K. M.; Scott, J. F. Physics of Thin-film Ferroelectric Oxides. *Rev. Mod. Phys.* **2005**, *77*, 1083−1130.
(4) Yamada, H.; Garcia, V.; Fusil, S.; Boyn, S.; Marinova, M.; Gloter, A.; Xavier, S.; Grollier, J.; Jacquet, E.; Carretero, C.; Deranlot, C.; Bibes, M.; Barthelemy, A. Giant Electroresistance of Super-tetragonal $BiFeO_3$-based Ferroelectric Tunnel Junctions. *ACS Nano* **2013**, *7*, 5385−5390.
(5) Ji, W.; Yao, K.; Liang, Y. C. Bulk Photovoltaic Effect at Visible Wavelength in Epitaxial Ferroelectric $BiFeO_3$ Thin Films. *Adv. Mater.* **2010**, *22*, 1763−1766.
(6) Ederer, C.; Spaldin, N. A. Effect of Epitaxial Strain on the Spontaneous Polarization of Thin Film Ferroelectrics. *Phys. Rev. Lett.* **2005**, *95*, 257601.
(7) Zeches, R. J.; Rossell, M. D.; Zhang, J. X.; Hatt, A. J.; He, Q.; Yang, C. H.; Kumar, A.; Wang, C. H.; Melville, A.; Adamo, C.; Sheng, G.; Chu, Y. H.; Ihlefeld, J. F.; Erni, R.; Ederer, C.; Gopalan, V.; Chen, L. Q.; Schlom, D. G.; Spaldin, N. A.; Martin, L. W.; Ramesh, R. A Strain-Driven Morphotropic Phase Boundary in $BiFeO_3$. *Science* **2009**, *326*, 977−980.
(8) Zhang, J. X.; Xiang, B.; He, Q.; Seidel, J.; Zeches, R. J.; Yu, P.; Yang, S. Y.; Wang, C. H.; Chu, Y. H.; Martin, L. W.; Minor, A. M.; Ramesh, R. Large Field-Induced Strains in a Lead-free Piezoelectric Material. *Nat. Nanotechnol.* **2011**, *6*, 98−102.
(9) Chen, Z.; Luo, Z.; Qi, Y.; Yang, P.; Wu, S. Low Symmetry Monoclinic M_C Phase in Epitaxial $BiFeO_3$ Thin Films on $LaSrAlO_4$ Substrates. *Appl. Phys. Lett.* **2010**, *97*, 242903.
(10) Béa, H.; Dupe, B.; Fusil, S.; Mattana, R.; Jacquet, E.; Warot-Fonrose, B.; Wilhelm, F.; Rogalev, A.; Petit, S.; Cros, V.; Aname, A.; Petroff, F.; Bouzehouane, K.; Geneste, G.; Dkhil, B.; Lisenkov, S.; Ponomareva, I.; Bellaiche, L.; Bibes, M.; Barthelemy, A. Evidence for Room-Temperature Multiferroicity in a Compound with a Giant Axial Ratio. *Phys. Rev. Lett.* **2009**, *102*, 217603.
(11) Zhang, J. X.; He, Q.; Trassin, M.; Luo, W.; Yi, D.; Rossell, M. D.; Yu, P.; You, L.; Wang, C. H.; Kuo, C. Y.; Heron, J. T.; Hu, Z.; Zeches, R. J.; Lin, H. J.; Tanaka, A.; Chen, C. T.; Tjeng, L. H.; Chu, Y. H.; Ramesh, R. Microscopic Origin of the Giant Ferroelectric Polarization in Tetragonal-like $BiFeO_3$. *Phys. Rev. Lett.* **2011**, *107*, 147602.
(12) Mazumdar, D.; Shelke, V.; Iliev, M.; Jesse, S.; Kumar, A.; Kalinin, S. V.; Baddorf, A. P.; Gupta, A. Nanoscale Switching Characteristics of Nearly Tetragonal $BiFeO_3$ Thin Films. *Nano Lett.* **2010**, *10*, 2555−2561.
(13) Ricinschi, D.; Yun, K. Y.; Okuyama, M. A Mechanism for the 150 $\mu C/cm^2$ Polarization of $BiFeO_3$ Films Based on First-Principles Calculations and New Structural Data. *J. Phys.: Condens. Matter* **2006**, *18*, L97−L105.
(14) Liu, H.; Yang, P.; Yao, K.; Ong, K. P.; Wu, P.; Wang, J. Origin of a Tetragonal $BiFeO_3$ Phase with a Giant c/a Ratio on $SrTiO_3$ Substrates. *Adv. Funct. Mater.* **2012**, *22*, 937−942.
(15) Belik, A. A.; Rusakov, D. A.; Furubayashi, T.; Takayama-Muromachi, E. $BiGaO_3$-based Perovskites: A Large Family of Polar Materials. *Chem. Mater.* **2012**, *24*, 3056−3064.
(16) Yan, J.; Gomi, M.; Yokota, T.; Song, H. Phase Transition and Huge Ferroelectric Polarization Observed in $BiFe_{1-x}Ga_xO_3$ Thin Films. *Appl. Phys. Lett.* **2013**, *102*, 222906.
(17) Zhao, Y. J.; Yin, Z. G.; Zhang, X. W.; Fu, Z.; Sun, B. J.; Wang, J. X.; Wu, J. L. Heteroepitaxy of Tetragonal $BiFeO_3$ on Hexagonal Sapphire(0001). *ACS Appl. Mater. Interfaces* **2014**, *6*, 2639−2646.
(18) King-Smith, R. D.; Vanderbilt, D. Theory of Polarization of Crystalline Solids. *Phys. Rev. B* **1993**, *47*, 1651−1654.
(19) Vanderbilt, D.; King-Smith, R. D. Electric Polarization as a Bulk Quantity and Its Relation to Surface Charge. *Phys. Rev. B* **1993**, *48*, 4442−4455.
(20) Gonze, X.; Allan, D. C.; Teter, M. P. Dielectric Tensor, Effective Charges, and Phonons in α-Quartz by Variational Density-Functional Perturbation Theory. *Phys. Rev. Lett.* **1992**, *68*, 3603−3606.
(21) Baroni, S.; Resta, R. *Ab Initio* Calculation of the Macroscopic Dielectric Constant in Silicon. *Phys. Rev. B* **1986**, *33*, 7017−7021.

DOI: 10.1021/am509016w
ACS Appl. Mater. Interfaces 2015, 7, 2648−2653